Black Hole Mass and Eddington Ratio as Drivers for the Observable Properties of Radio-Loud and Radio-Quiet QSOs

Todd A. Boroson

National Optical Astronomy Observatory, P.O. Box 26732, Tucson, AZ 85726-6732

ABSTRACT

Recent studies of black holes in the nuclei of both active and normal galaxies have yielded relationships that permit a physical interpretation of the principal components of the spectra of QSOs. It is shown that principal component (or eigenvector) 1 (PC1) is driven predominantly by L/L_{Edd}, and principal component 2 (PC2) is driven by accretion rate. This results in a PC2 vs. PC1 diagram in which lines of constant black hole mass are diagonal. Using a sample consisting of the low-redshift PG objects supplemented by 75 radio-loud QSOs, it is shown that such a diagram effectively distinguishes radio-loud from radio-quiet objects as well as demonstrating that both narrow-line Seyfert 1s and broad absorption-line QSOs lie at the high L/L_{Edd} extreme, though these two types of objects are well separated in the PC2 direction. A simple picture that ties together physical parameters (black hole mass and Eddington ratio) and classification of AGN is presented. Based on the location of core-dominated and lobe-dominated radio-loud QSOs, orientation can be modeled as a third parameter in this scheme, implying an enhancement in the radio flux of core-dominated objects.

Subject headings: galaxies: Seyfert—galaxies: nuclei—quasars: general

1. Introduction

Recent studies have derived black hole masses for normal and active galactic nuclei and have attempted to relate them to observable properties. Perhaps the most striking of these relations is the discovery that the nuclear black hole mass in normal galaxies is tightly correlated with σ^n, where σ is the velocity dispersion of the bulge of the host galaxy and n is in the range 3.75 to 4.8 (Gebhardt et al. 2000; Ferrarese and Merritt 2000). Although the distances to even the nearest QSOs preclude the spatially resolved spectroscopy that is the basis for determination of black hole masses for normal galaxies, other techniques (e.g., reverberation mapping), as well as the presumed extension of the relation between black hole

mass and host galaxy bulges, permit the comparison of physical parameters with observable properties for active galactic nuclei.

?)BG92]BG92 showed that most of the variance in the measured optical emission-line properties and a broad range of continuum properties (radio through x-ray) in a complete sample of low-redshift QSOs was contained in two sets of correlations, eigenvectors of the correlation matrix. Principal component 1 (PC1) links the strength of Fe II emission, [O III] emission, and $H\beta$ line asymmetry. Principal component 2 (PC2) projects most strongly on optical luminosity and the strength of He II λ4686 emission. Subsequent studies (see Sulentic et al. (2000) and references therein) have added observed properties to the list, and have, in general, confirmed the reality of the correlations.

BG92 and others since have tried to understand the relationship between the principal components and the physical parameters that govern the energy-producing and radiation-emitting processes. As the summary presentation in a conference titled: "Structure and Kinematics of Quasar Broad Line Regions", Gaskell (1999) polled the conference attendees on the question "What drives Boroson-Green Eigenvector 1?" The overwhelming consensus was "Don't Know", which received 68% of the votes.

Of course, the eigenvectors are merely a mathematical construct to describe and to reduce the dimensionality of the object-to-object variations. They are orthogonal by definition, but their relationship to real physical properties may be complex or non-existent. It is tempting, however, to use them and to explore their relationship to physical parameters because (a) by reducing the dimensionality they allow models to be parameterized in simpler ways, (b) they link together diverse properties and provide more robust tests of such models, (c) they increase the "signal-to-noise" by allowing the merging of multple samples.

By far the most popular interpretation has been that PC1 is highly correlated with L/L_{Edd}, the Eddington ratio. This was put forward by BG92 as the basis for a picture in which the vertical structure of the accretion disk, governed by the Eddington ratio, drives line strengths and continuum components through its illumination of broad-line clouds and an extended narrow-line region. Other factors which have been discussed as possibly playing a role in the properties that PC1 comprises are black hole spin and orientation.

In this paper, we explore the relation between the principal components that describe the observed properties and determinations of the physical properties. We begin by reviewing the observed correlations, including a simple visualization of the PC1 and PC2 sequences in Section 2. In Section 3, we adopt from the literature methods for determining the physical properties and attempt to understand PC1 and PC2 in terms of these. In Section 4, these relations are extended to include new samples of radio-loud objects, and it is demonstrated

that a consistent picture of the relation between observables and physical properties emerges. In Section 5, this picture is further explored as a context for the classification of QSOs, including the expected effects of orientation. Conclusions are summarized in Section 6.

2. The Two Principal Components

BG92 obtained spectra covering the region $\lambda\lambda 4300 - 5700$ for all 87 QSOs in the BQS catalog having redshifts less than 0.5. Measurements of the strengths of Fe II, $H\beta$, [O III]λ5007, He IIλ4686, were combined with a four-dimensional parameterization of the Hβ line and broad-band continuum information, including M_V, α_{ox}, and log R, the ratio of radio-to-optical flux density. Principal component analysis performed on this dataset yielded the result that most of the variance in the tabulated line and continuum properties was contained in two principal components or eigenvectors, which we call PC1 and PC2.

PC1 is dominated by the inverse correlation between the strengths of Fe II and [O III]. Objects that have strong Fe II and weak [O III] also tend to be radio quiet, and to have $H\beta$ lines that are narrower and blue asymmetric (more flux on short wavelength shoulder of the line). Objects that have weak Fe II and strong [O III] tend to be radio loud (though not exclusively), and to have $H\beta$ lines that are broader and red asymmetric. Note that none of these properties is completely correlated with PC1; although all of the extreme Fe II-weak/[O III]-strong objects are radio-loud, for example, about half of the radio-loud objects are mixed with radio-quiet objects in the same half of the PC1 distribution.

PC2 is dominated by luminosity and its anticorrelation with the strength of He II. There is also a moderately strong relation with α_{ox} such that lower luminosity objects (which have strong He II emission) rise more steeply from their optical continuum into the x-rays.

For this study, the principal component analysis of BG92 has been repeated, using updated measurements of a few of the observables. All the α_{ox} values fom BG92 have been replaced with those given by Brandt, Laor, and Wills (2000). Two incorrect $H\beta$ FWHM values have been replaced: PG 1307+085 (5320 km/s) and PG 2304+042 (6500 km/s) (Laor 2000). Also, PG 1211+143 has been changed from radio-loud to radio-quiet (Kellerman et al. 1994). The variable that was called Peak λ5007, a measure of the relative heights of the peaks of the [O III] and $H\beta$ lines, has been replaced with a variable that is less dependent on the resolution of the observation. The new Peak λ5007, designated Peak2 λ5007, is given by EW λ5007 / EW $H\beta \times H\beta$ FWHM / 1000. This has characteristics quite similar to Peak λ5007 (correlation coefficient r = 0.91 between the two variables), but can be determined consistently and accurately from observations with other instruments.

The principal component analysis was carried out using Vista, a freeware package written and distributed by Dr. Forrest Young of the University of North Carolina, Department of Psychology (http://www.visualstats.org). The principal components that emerged from this analysis are very similar to those found by BG92. Figure 1 presents the distribution of the 87 low-redshift PG objects in the new PC1-PC2 space, with different symbols used for narrow-line Seyfert 1's (NLS1s; solid circles), broad absorption-line QSOs (BALQSOs; solid triangles), other radio-quiet (solid squares), flat-spectrum radio-loud (open triangles), and steep-spectrum radio-loud (open circles) objects. Because the PG sample has a high incidence of relatively narrow line objects, a more restrictive definition of a NLS1 is used: having Hβ FWHM < 1500 km s^{-1} rather than the usual limit of 2000 km s^{-1}.

Table 1 gives information for evaluating PC1 and PC2. Listed here are the variables used (see BG92 for definitions), the mean and standard deviation for each variable in the PG sample, and the coefficients. The PC1 and PC2 values are given by the linear combination of the normalized variables: $PC1 = \sum c_{1,i}(x_i - \mu_i)/\sigma_i$ where $c_{1,i}$ is the coefficient for the ith variable and the first principal component, x_i is the measurement of the ith variable, and μ_i and σ_i are the mean and standard deviation of the ith variable.

It is interesting to note that although radio-loud objects are distinguished clearly by neither PC1 nor PC2, almost all of them fall in the lower right corner of the figure. Also note that BALQSOs and NLS1 objects both fall at the low PC1 end of the diagram, but at opposite ends of PC2. The four corner regions marked in Figure 1 serve to isolate the objects with extreme values of PC1 and PC2. In order to get a visual impression of the relationship between the principal components and the spectra, we have averaged the spectra of the objects in each of the corner regions. Figure 2 shows the average spectra of the objects in the four extreme regions.

It is also interesting that while the increase in He IIλ4686 strength is visible from bottom to top on the right hand (weak Fe II) side, it is also clearly present in the objects that have strong Fe II and weak [O III]. Figure 3 shows the very broad He IIλ4686 line that emerges when the spectra of the low PC1 high PC2 objects are averaged, but after removing Fe II and continuum contributions.

BG92 proposed that PC1 is related to the fraction of the Eddington luminosity at which the object is emitting. This speculation arose from a very qualitative picture of accretion disk structure and radiative transfer, in which, as the accretion rate increases to a value close to the Eddington limit, the disk puffs up vertically, supported by radiation pressure. The expected consequences of this include a large x-ray heated volume that could generate the Fe II emission, and substantial shielding of the extended narrow-line region from UV ionizing radiation, resulting in weaker [O III] emission. Subsequently, some support for this

explanation has been provided by studies (e.g., Brandt and Boller (1999)) of NLS1s, which lie at one extreme of PC1. These objects show a strong soft x-ray excess, which is attributed to thermal emission from a viscously-heated accretion disk that results at an accretion rate close to the Eddington limit (Pounds, Done, and Osborne 1995). PC2 is presumably related predominantly to the accretion rate itself, since it is strongly correlated with the optical luminosity.

3. Black Hole Masses

While the masses of black holes in active galaxies have not yet been determined through the spatially resolved spectroscopy that provides the most convincing measurements for nearby non-active galaxies, a number of studies have explored derivative methods. Mcleod and McLeod (2001) and McLeod, Rieke, and Storrie-Lombardi (1999) use the assumption that the black hole mass is a constant fraction of the bulge luminosity and show that sensible fractions (a few percent to a few tens of percent) of the Eddington luminosity result. Kaspi et al. (2000) and McLure and Dunlop (2001) use reverberation mapping to determine the radius of the emitting material and then use emission line widths to estimate the black hole mass. The samples used in these studies are small but there is some overlap with the BG92 sample.

A number of studies (Kaspi et al. (1996), Laor (1998), McLure and Dunlop (2001), Merritt and Ferrarese (2001)) have developed formalisms that relate the black hole mass to the emission line width and some measure of the luminosity through the assumption that the BLR clouds' motion is virialized and using the relationship between R_{BLR} and luminosity found by Kaspi et al. (1996) from reverberation mapping. Although this approach no doubt represents a simplified view of the relationships, it has the advantage that it provides a uniform and consistent estimate of black hole mass from a sample that has uniform and consistent measturements of the input parameters. For this study, we adopt the assumptions and parameters advocated by Merritt and Ferrarese (2001): $R_{BLR} = 32.9(\lambda L_{5100}/10^{44} ergs^{-1})^{0.7}$ light days (Kaspi et al. 2000) and $v_{BLR} = \sqrt{3}/2 FWHM(H\beta)$. Using the BG92 $H\beta$ FWHM values and the Neugebauer et al. (1987) spectrophotometry in these formulae, black hole masses can be computed for all 87 objects in the BG92 sample.

We now would like to test whether any relationship exists between the principal components of the PG dataset and the values of M_{BH} and L/L_{Edd} derived in this way. Because the prescription for M_{BH} and L/L_{Edd} use v_{BLR} and L_{5100}, which are derived from (or highly correlated with) $H\beta$ FWHM and M_V respectively, we perform two additional principal component analyses, one excluding $H\beta$ FWHM as an input variable and one excluding both $H\beta$

FWHM and M_V as input variables. Note that $H\beta$ FWHM but not M_V figure prominently in the first principal component, the one that we suspect is driven by L/L_{Edd}. Table 2 gives the correlation coefficients among L/L_{Edd}, M_{BH}, and the two principal components of each of the three analyses. It is clear that L/L_{Edd} is most highly correlated with PC1; correlation coefficients of 0.53, 0.45, and 0.45 are found for the three analysis. These correspond to chance probabilities less than 0.01%. Note also that M_{BH} is highly correlated with both principal components.

4. Enlargement of the sample

The PG sample, although well defined, contains only a small number of radio-loud QSOs. In order to work with a sample that will allow conclusions to be drawn about the differences between radio-quiet and radio-loud objects, we supplement the BG92 measurements with two radio-loud samples, 46 objects from Corbin (1997) and 29 additional objects from Brotherton (1996). A few of the objects from those samples in which the S/N was obviously poor, or in which [O III] λ5007 could not be accurately measured were excluded. Measurements of the emission-line parameters including the strengths of $H\beta$, [O III] λ5007, and Fe II and the width, shape, shift, and asymmetry of $H\beta$ are drawn from those papers. Continuum properties such as M_V, α_{ox}, and log R are drawn from those papers or references therein. In a few cases, we have updated these values or filled in missing values through searches of the more recent literature.

Having tabulated the known values for these 75 additional objects, the approach taken toward combining the samples was not to repeat the PCA with the entire dataset. Because the new objects represent very different selection criteria than the original PG sample, the variance in the total sample would be dominated by the differences between the original UV-excess selected objects that are predominantly radio-quiet and of lower luminosity and the new radio-selected objects that are at somewhat higher redshift and higher luminosity. The goal of increasing the sample is to use the tools that have been derived from the PG analysis to better understand what happens when the extent of parameter space is increased. Therefore, the projections of the new objects on the principal components derived in the previous section were evaluated (using the coefficients given in Table 1) and the new PC1 vs. PC2 diagram is shown in Figure 4.

In evaluating the new objects in terms of the original principal components, some of the variables that are elements of the definitions of the principal components were not measured. Specifically, none of the new objects have measurements of the equivalent width of He II λ4686, and some do not have measurements of Fe II, α_{ox}, $H\beta$ shift, or $H\beta$ shape. In these

cases, a conservative approach was used. It was assumed that the missing value was equal to the mean value of the PG sample. This has the effect of eliminating any influence that a missing variable would have on the position of the object in PC1-PC2 space. Another possible approach would have been to use the established correlations between variables with missing values and other variables in order to estimate the missing values. This might, however, have the effect of unrealistically exaggerating any distinctions between the radio-loud and radio-quiet objects, and so the more conservative approach was adopted.

Figure 4 shows a dramatic difference between the positions of radio-loud (open symbols) and radio-quiet (solid symbols) objects. With almost no overlap, the two sets of objects (including on the radio side both steep-spectrum and flat-spectrum objects) can be divided by a straight line, drawn by eye as a dashed line in figure 4.

Because log R, the ratio of radio to optical flux density is a contributor to the principal components, one might imagine that it is the very fact that the radio-loud objects have large log R that is moving them to the lower right part of the PC1-PC2 diagram. To test this, the projections of the objects on the principal components was reevaluated, this time with no contribution from log R. These "radio-free" values are shown in figure 5. As expected, the radio-loud objects have moved up and to the left, but not nearly far enough to eliminate the distinction between radio-loud and radio-quiet. The same dashed line as in figure 4 is shown in figure 5 for reference.

What physical parameter causes this separation? By using $H\beta$ FWHM and optical luminosity to compute M_{BH} for the PG sample, Laor (2000) finds that radio-loud QSOs are associated with the most massive black holes. This result has been confirmed and refined by Lacy et al. (2001) who added a radio-selected sample to the PG objects. Lacy et al. (2001) find that radio luminosity scales proportional to $M_{BH}^{1.9}(L/L_{Edd})^{1.0}$.

Using the same approach as Laor (2000), the black hole masses for this sample can be evaluated. These are shown by the color coding of the points in the PC1-PC2 plane in figure 6. The objects have been binned in ranges of 0.5 in log M_{BH} and the average positions of all objects in each of those bins are shown as the large colored plus signs in figure 6. It is clear that the trend in M_{BH} parallels the trend in radio loudness. This is exactly the expectation, of course, if PC1 is driven primarily by L/L_{Edd} (proportional to L/M) and PC2 is driven primarily by accretion rate (proportional to L).

In addition to the trend of increasing black hole mass from upper left to lower right, another striking feature of figure 6 is that the transition between radio-quiet and radio-loud objects is much more sharply defined than are the black hole mass bins. Thus, both the cyan and magenta objects ($9.0 < \log M_{BH} < 10.0$) appear to span the dividing line between

radio-quiet and radio-loud. One possible explanation for this is that the PC1-PC2 plane provides a superior method for determining black hole mass than does the simple formula that uses only Hβ FWHM and luminosity. Another possibility, though, is that there is a correlation between the radio emission itself and one or more of the other properties that consitute the principal components. For example, it is possible that radio jets trigger star formation which produces an enhanced level of [O III] emission. A test for this would be to compare the [O III] emission strength for radio-loud and radio-quiet objects with the same Fe II emission strength. Such a test shows no difference in [O III] between the two groups, however.

5. Discussion: A Paradigm for AGN classification

Figure 6 suggests a relatively simple diagram, shown in figure 7, that links together physical properties and observables. This diagram, which provides a physical basis for classification of different types of AGNs, something like an HR diagram does, plots luminosity or accretion rate against Eddington ratio. The observational analogs of these properties are PC2 and PC1. Note that the theoretical quantities are not orthogonal but are related linearly, although PC2 and PC1 are orthogonal mathematically within the PG sample. Lines of constant black hole mass are diagonal lines in this diagram.

The extreme regions along both axes may be restricted because of either physical constraints (e.g., difficulty in accreting above the Eddington limit) or observational constraints (e.g., too low a luminosity will preclude classification as an AGN). Within the allowed region it can be seen that radio loud QSOs will be found predominantly in elliptical galaxies, systems hosting black holes of greater mass, while radio-quiet QSOs will be found in lower mass spheroidal systems – i.e., generally spirals – as they have lower mass black holes. The most extreme low black hole mass objects are the NLS1s, falling at the upper left of the PC1-PC2 diagram.

BALQSOs apparently fall at the lower left corner, that is, high Eddington ratio and high luminosity. Since this position is near the dividing line between radio-loud and radio-quiet, one could conjecture that radio-loud BALQSOs would have extremely high luminosity, causing them to fall below that dividing line. This is consistent with the most promising candidates for radio-loud BALQSOs, such as FIRST J155633.8+351758 (Najita, Dey, and Brotherton 2000). Thus, the scarcity of radio-loud BAL QSOs would be due to the relatively small region of parameter space that is available when an object is to be a BAL (high Eddington ratio, high accretion rate) and radio-loud (large black hole mass).

As noted by Laor (2000), it might be expected that three parameters, black hole mass, Eddington ratio, and orientation, would determine the observable characteristics of AGNs. While the picture developed in this paper includes the first two, there has been little indication of anything that could be interpreted as orientation. This is, in some sense, in conflict with the "standard unification model" in which orientation plays a major role in providing context for the classification of AGNs (Antonucci 1993; Urry and Padovani 1995). The unification model, based on the ideas of relativistically beamed emission and a thick (vertically and optically) torus, receives support from scattered broad line emission seen in some Seyfert 2 galaxies, the "alignment effect" seen in high redshift radio galaxies, as well as a number of consistency arguments applied to various statistical samples.

Within the samples considered in this study, the most obvious groups to explore for orientation effects are the core-dominated (flat-spectrum) and lobe-dominated (steep-spectrum) radio-loud QSOs. It has been conjectured that if a radio-loud QSO is seen along its jet, it will appear as a core-dominated source, with the core radio emission enhanced by relativistic beaming. If the jet is close to the plane of the sky, however, the lobes will dominate, and will be well apart from the cental source. Studies comparing the two types suffer from the difficulty of picking samples that include objects of similar intrinsic properties.

Although Figure 6 shows little obvious separation between the core-dominated (open triangles) and lobe-dominated (open circles) objects, a Kolmogrov-Smirnov test indicates a significant difference (chance probability $< 0.5\%$) in the distribution of PC1, with core-dominated objects having lower values of PC1 by about 1.0 in the median than lobe-dominated objects. Of course, log R is a component of PC1 (as log R increases, PC1 increases), but the median log R value for the core-dominated objects is larger than that of the lobe-dominated objects: 3.14 as opposed to 2.56 No significant difference is seen in PC2.

What would be expected? If core-dominated objects have weaker intrinsic radio luminosity but their emission is enhanced by beaming and if the orientation has no effect on any property other than log R used in our analysis, then this is qualitatively a consistent finding. Within this simplistic picture, an enhancement of 2.8 in log R is required to explain the location of the core-dominated objects. This is extremely speculative as it depends on (a) unquantifiable selection effects in the samples considered here, (b) unknown additional effects that orientation might have on other properties that went into the analysis, and (c) a derivation of principal components that was based on the assumption that the log R values of core- and lobe-dominated objects have the same intrinsic meaning.

6. Conclusions

A revised statistical analysis of the properties of the low-redshift PG QSOs has been performed, with updated measurements. Two principal components have been identified, corresponding, as in BG92, to the Fe II–[O III] anticorrelation and to the luminosity. Black hole masses for this sample have been estimated using the formula derived by Laor (2000). These indicate that the two principal components correspond closely to the Eddington ratio and the accretion rate, respectively. Two additional radio-loud samples have been added to the analysis, by using the principal component definitions derived from the PG sample. Inspection of the PC1-PC2 diagram for this enlarged sample shows that:

1. Diagonal lines in the PC1-PC2 diagram represent lines of constant black hole mass.
2. Radio-loud and radio-quiet objects are well separated by such a line, indicating that radio-loudness is determined by black hole mass.
3. NLS1s lie at the corner of the diagram indicative of having the lowest black hole masses.
4. BAL QSOs lie in the high Eddington ratio, high accretion rate corner of the diagram, suggesting that the rare radio-loud BAL QSOs must have extremely high accretion rates.
5. Comparison of the location of core-dominated and lobe-dominated radio-loud QSOs suggests that orientation manifests itself as a shift in PC1, perhaps due primarily to relativistic beaming of radio emission. With this assumption, an enhancement factor of 2.8 in the log is derived.

I wish to thank Richard Green and Michael Brotherton for helpful discussions, and Ari Laor for the use of his database. This research has made use of the NASA/IPAC Extragalactic Database (NED) which is operated by the Jet Propulsion Laboratory, California Institute of Technology, under contract with the National Aeronautics and Space Adminsitration.

REFERENCES

Antonucci, R. 1993, ARA&A, 31, 473.

Boroson, T.A. and Green, R.F. 1992, ApJS, 80, 109

Brandt, W.N. and Boller, T. 1999, in ASP Conf. Ser. 175, Structure and Kinematics of Quasar Broad Line Regions, ed. C. M. Gaskell, W.N. Brandt, M. Dietrich, D. Dultzin-Hacyan, and M. Eracleous (San Francisco: ASP), 265

Brandt, W.N., Laor, A., and Wills, B.J. 2000, ApJ, 528, 637

Brotherton, M.S. 1996, ApJS, 102, 1

Corbin, M.R. 1997, ApJS, 113, 245

Ferrarese, L., and Merritt, D. 2000, ApJ, 539, L9

Gaskell, C. M. 1999, in ASP Conf. Ser. 175, Structure and Kinematics of Quasar Broad Line Regions, ed. C. M. Gaskell, W.N. Brandt, M. Dietrich, D. Dultzin-Hacyan, and M. Eracleous (San Francisco: ASP), 423

Gebhardt, K., Bender, R., Bower, G., Dressler, A., Faber, S.M., Filippenko, A.V., Green, R., Grillmair, C., Ho, L.C., Kormendy, J., Lauer, T.R., Magorrian, J., Pinkney, J., Richstone, D., and Tremain, S. 2000, ApJ, 539, L13

Kaspi, S., Smith, P.S., Maoz, D., Netzer, H., and Jannuzi, B.T. 1996, ApJ, 471, L75

Kaspi, S., Smith, P.S., Netzer, H., Maoz, D., Jannuzi, B.T., and Giveon, U. 2000, ApJ, 533, 631

Kellerman, K.I., Sramek, R.A., Schmidt, M., Green, R.F., and Shaffer, D.B. 1994, AJ, 108, 1163

Lacy, M., Laurent-Muehleisen, S.A., Ridgway, S.E., Becker, R.H., and White, R.L. 2001, ApJ, 551, L17

Laor, A. 1998, ApJ, 505, L83

Laor, A. 2000, ApJ, 543, L111

McLeod, K.K. and McLeod, B.A. 2001, ApJ, 546, 782

Mcleod, K.K., Rieke, G.H., and Storrie-Lombardi, L.J. 1999, ApJ. 511, L67

McLure, R.J. and Dunlop, J.S. 2001, MNRAS, submitted (astro-ph/0009406)

Merritt, D. and Ferrarese, L. 2001, in ASP Conf. Ser. xxx, The Central kpc of Starbursts and AGN, ed., J.H. Knapen, J.E. Beckman, I. Shlosman, and T.J. Mahoney (San Francisco: ASP), in press.

Najita, J., Dey, A., Brotherton, M. 2000, AJ, 120, 2859

Neugebauer, G., Green, R.F., Matthews, K., Schmidt, M., Soifer. B.T., and Bennett, J. 1987, ApJS, 63, 615

Pounds, K.A., Done, C., and Osborne, J.P. 1995, MNRAS, 277, L5

Sulentic, J.W., Marziani, P., and Dultzin-Hacyan, D., ARA&A, 38 521

Sulentic, J.W., Zwitter, T., Marziani, P., Dultzin-Hacyan, D. 2000, ApJ, 536, L5

Urry, C.M. and Padovani, P. 1995, PASP, 107, 803

AAS LaTeX macros v5.0.

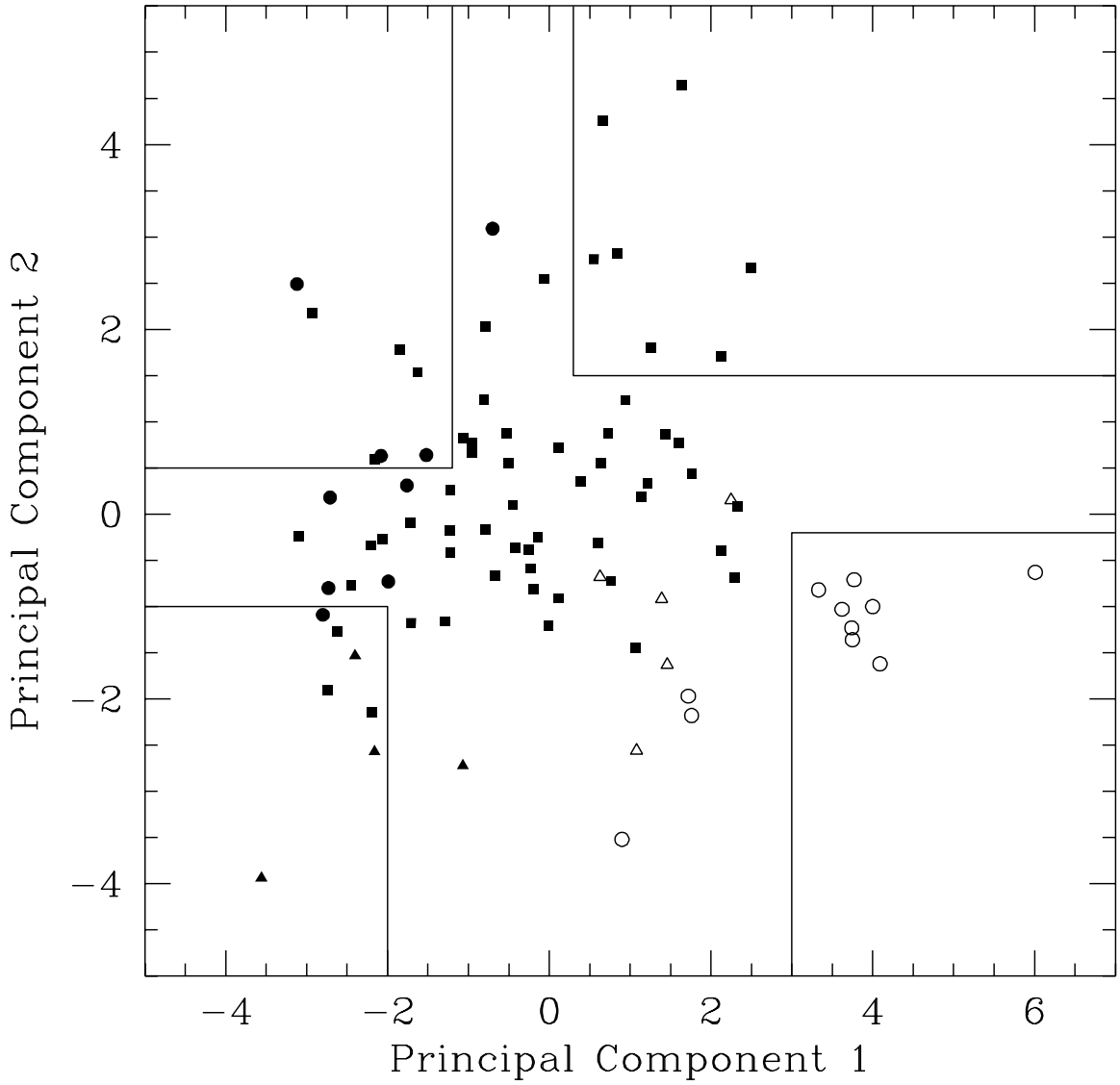

Fig. 1.— Distribution of the 87 low-redshift PG objects with respect to the two principal components. Symbols are solid triangles: BALQSOs, solid circles: NLS1s, solid squares: other radio quiet QSOs, open triangles: flat-spectrum radio-loud QSOs, and open circles: steep-spectrum radio-loud QSOs. The four marked off regions identify the objects whose spectra have been averaged to show the characteristics of the extremes of the two principal components.

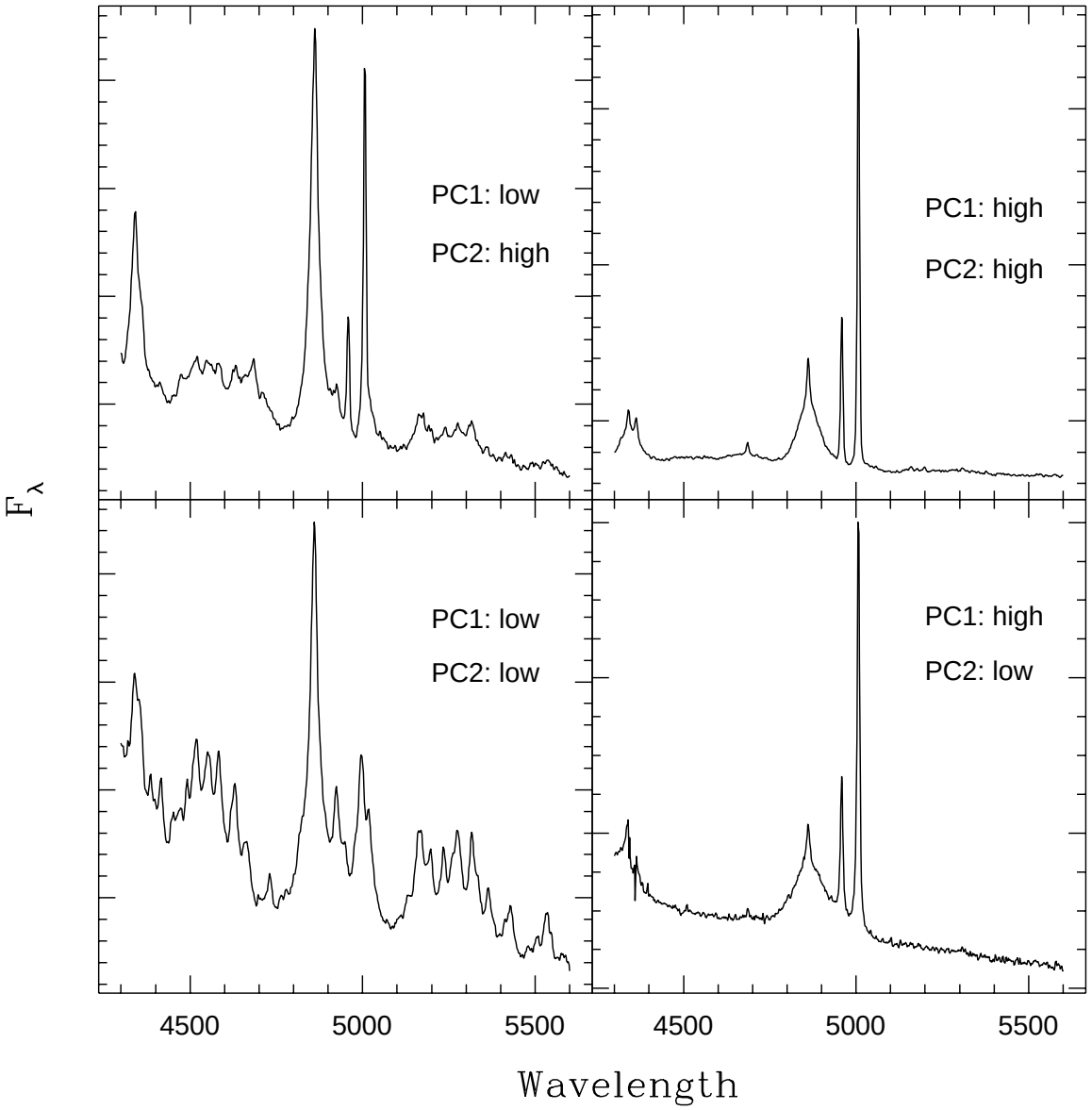

Fig. 2.— Average spectra of the PG objects having extreme values of the two prinicpal components. Each quadrant shows the average spectrum of the objects in the corresponding corner of figure 1.

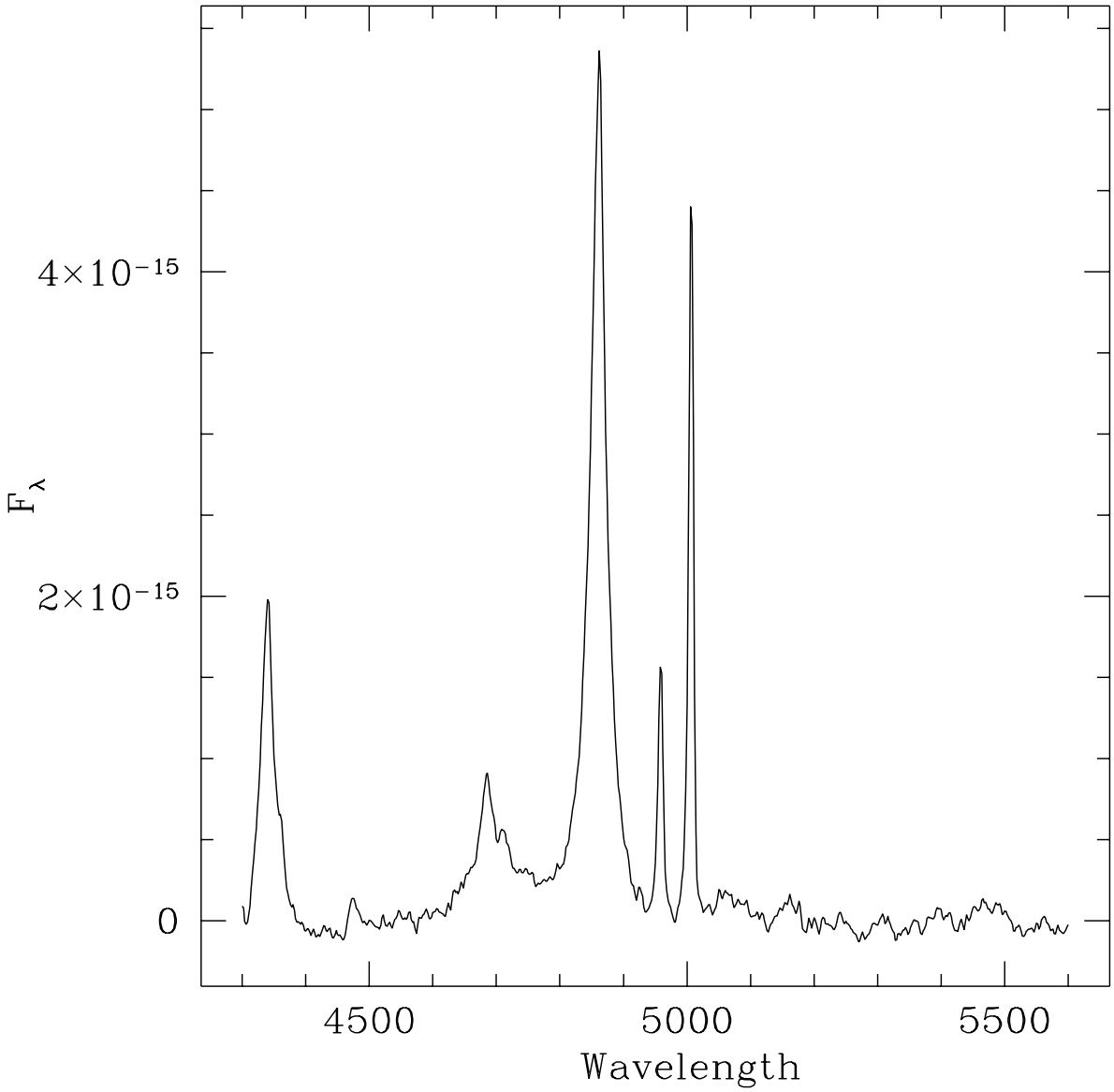

Fig. 3.— Average spectrum of the objects in the upper left (low PC1, high PC2) corner of figure 1, but with Fe II and continuum subtracted first. Note the strong, broad He II λ4686 emission line previously masked by the Fe II emission.

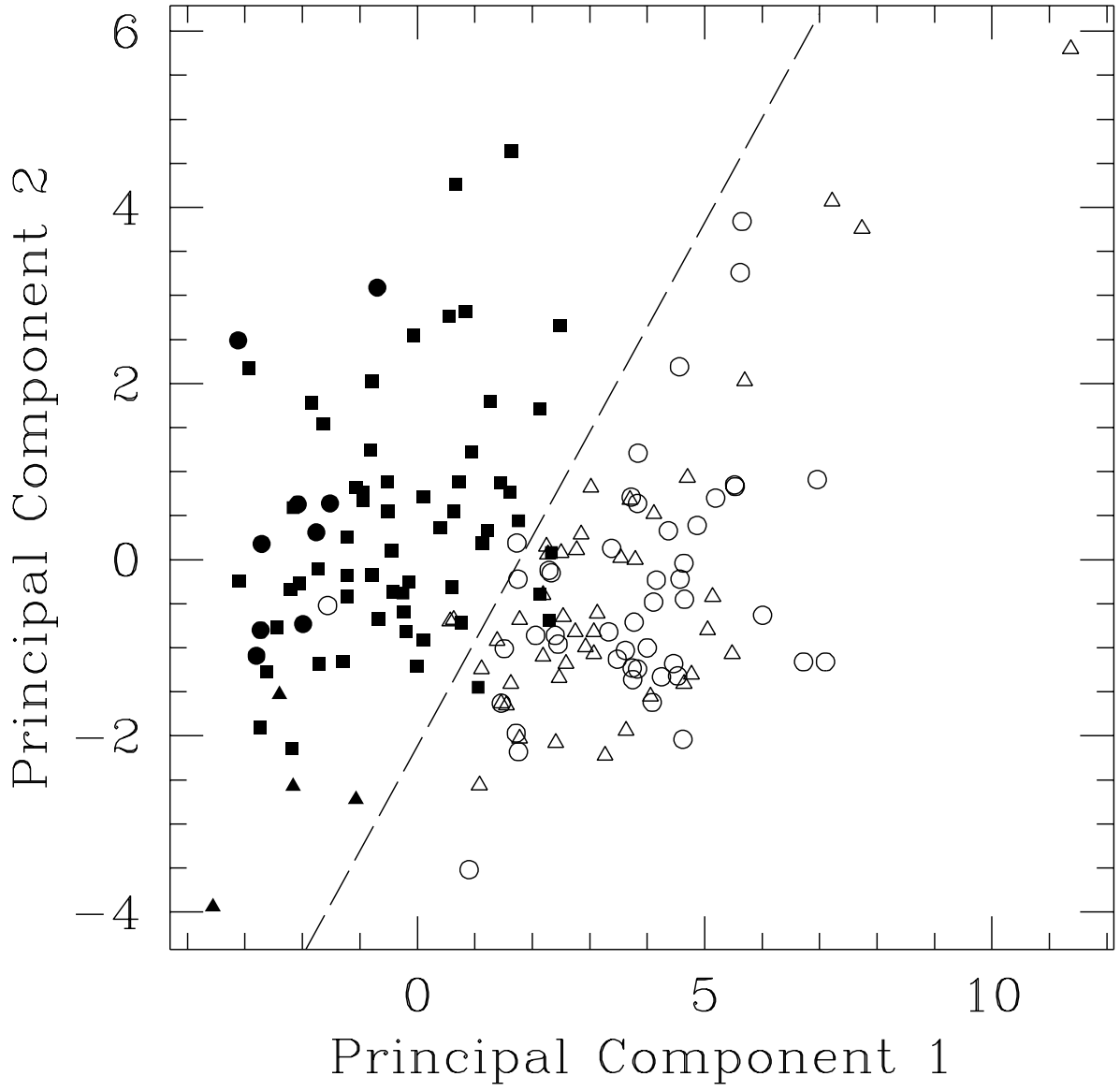

Fig. 4.— Distribution of the enlarged sample of 162 objects with respect to the two principal components. Symbols are solid triangles: BALQSOs, solid circles: NLS1s, solid squares: other radio quiet QSOs, open triangles: flat-spectrum radio-loud QSOs, and open circles: steep-spectrum radio-loud QSOs. The dashed line (drawn by eye) separates radio-loud and radio-quiet objects.

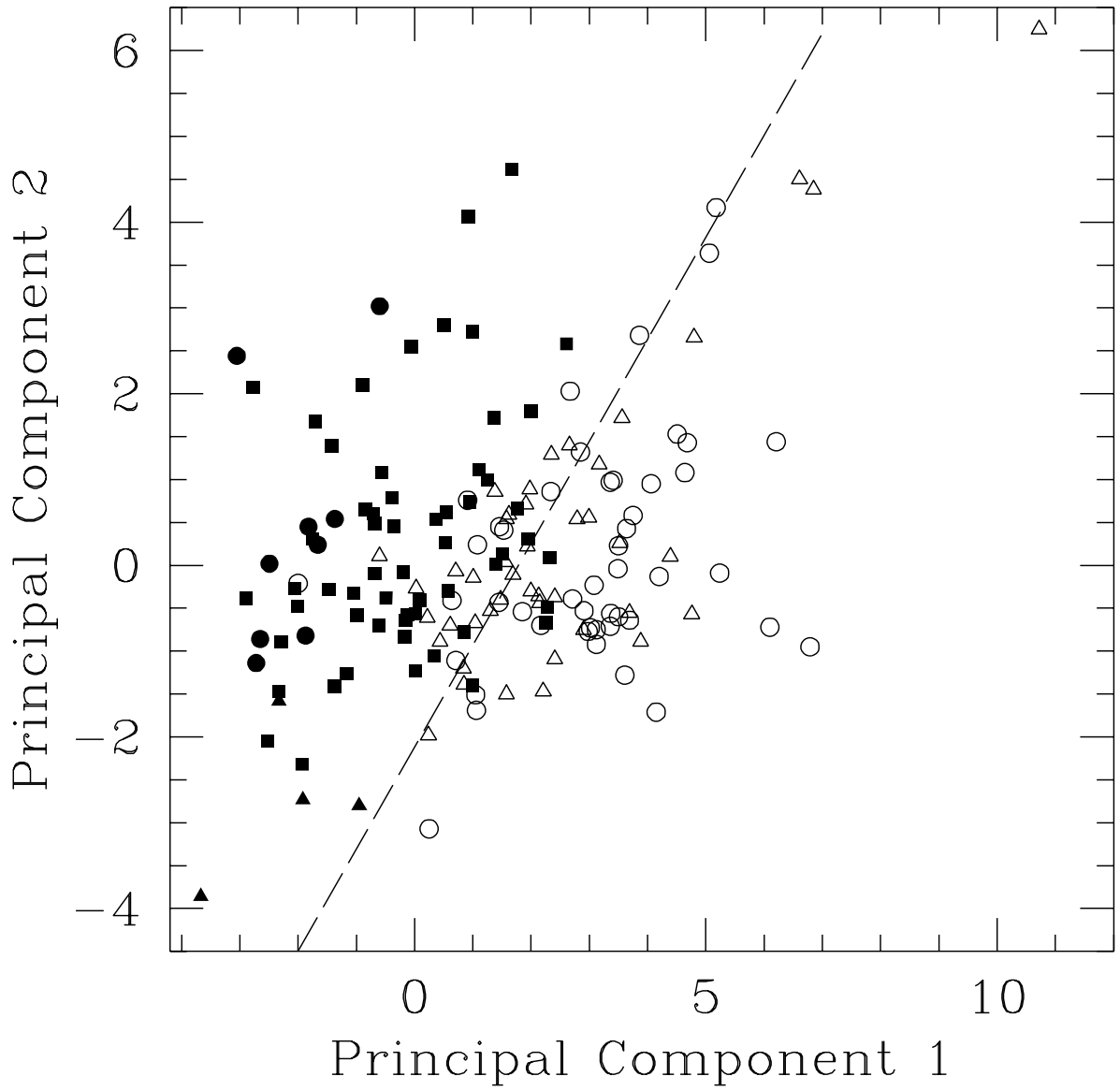

Fig. 5.— Same as figure 4 but with the effect of Log R removed from the principal components. Symbols are solid triangles: BALQSOs, solid circles: NLS1s, solid squares: other radio quiet QSOs, open triangles: flat-spectrum radio-loud QSOs, and open circles: steep-spectrum radio-loud QSOs. The dashed line is the same line as in figure 4, showing that the radio-loud objects have moved up and to the left, but are still well separated from the radio-quiet objects.

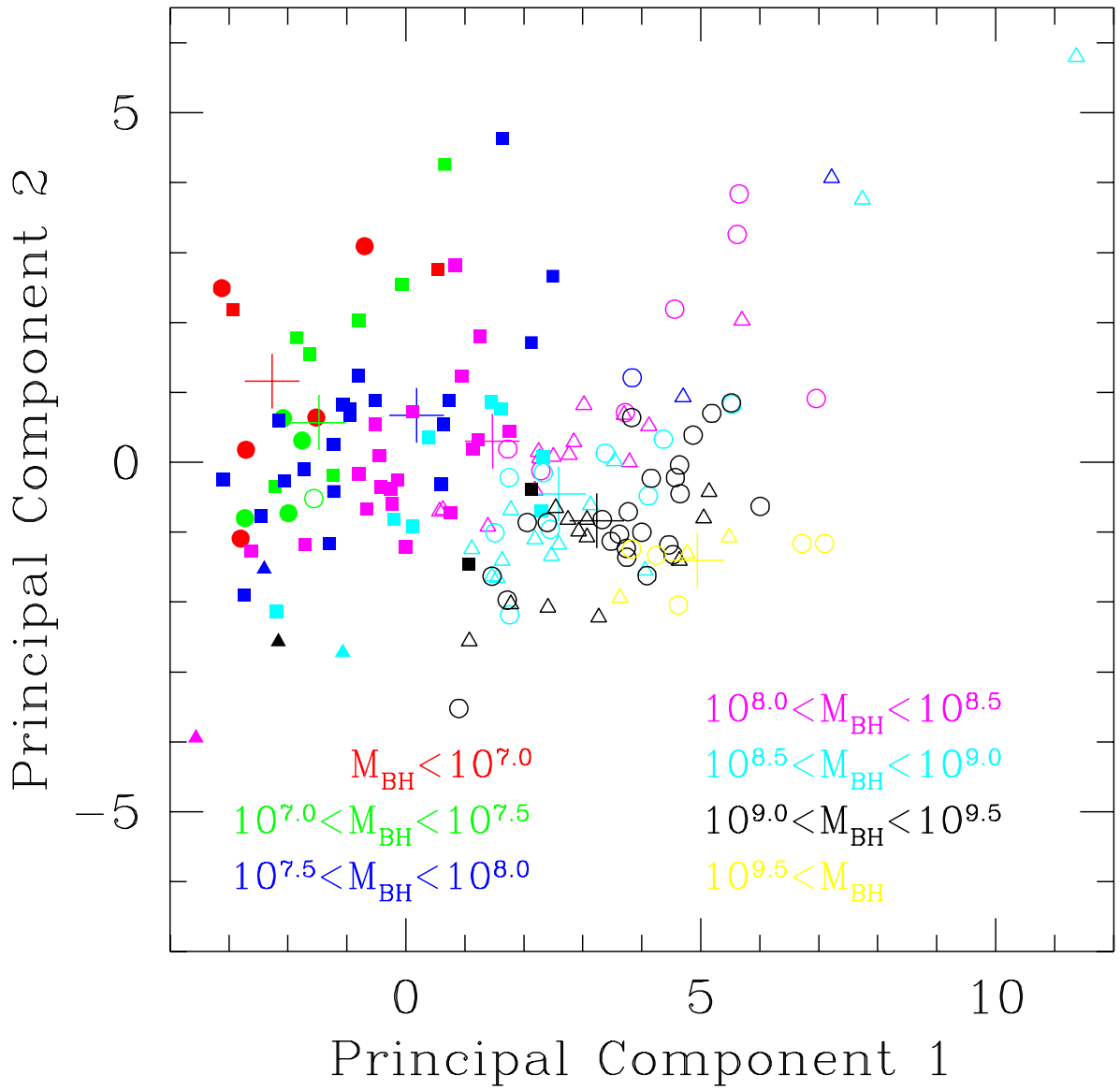

Fig. 6.— Distribution of objects in the PC1-PC2 plane, now color coded according to black hole mass as derived from the Merritt and Ferrarese (2001) formula. Symbols are as in figures 4 and 5. Range of black hole mass denoted by each color is given in legend at bottom. Large plus signs show average position of objects in each black hole mass bin.

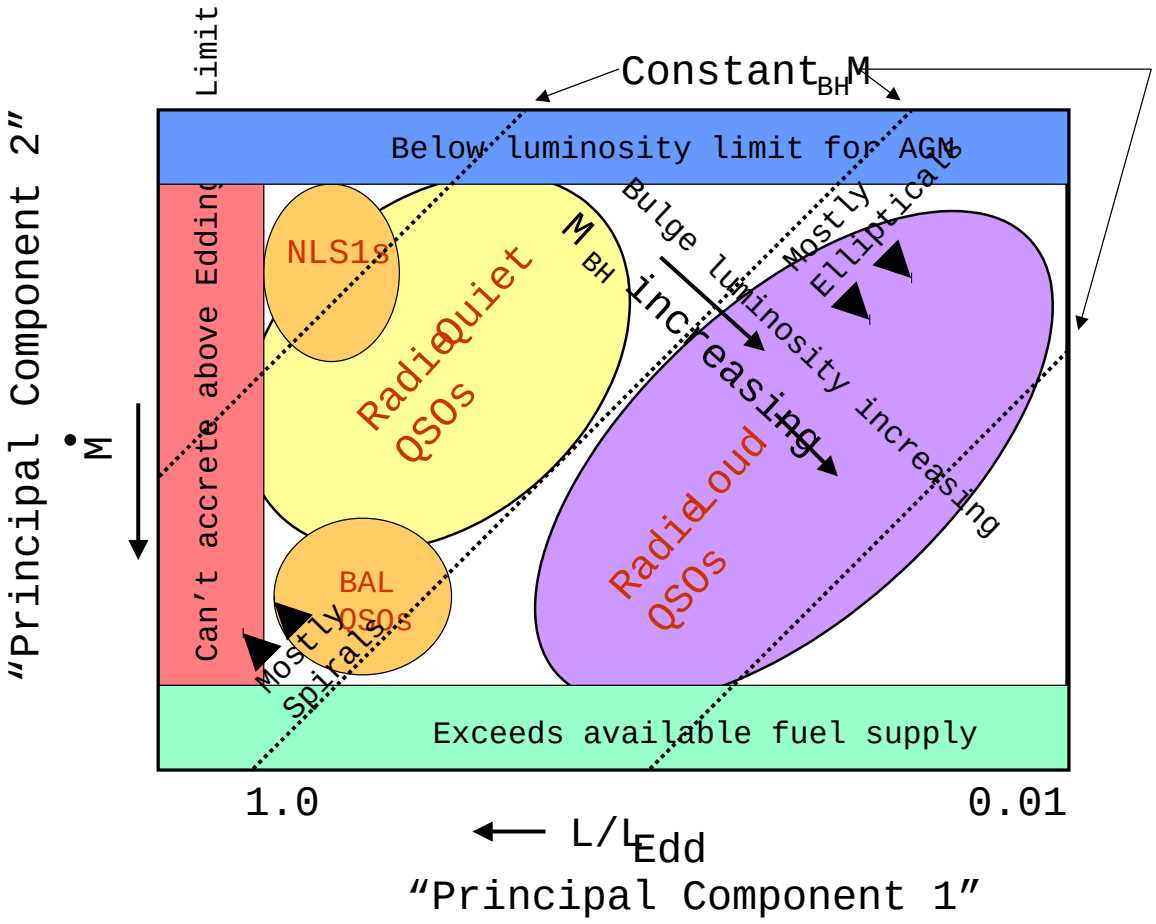

Fig. 7.— Interpretive diagram showing how PC1-PC2 plane provides basis for classification of AGNs.

Table 1. Coefficients for PC1 and PC2

Variable	Mean	Standard Deviation	Coefficient for PC1	Coefficient for PC2
M_V	−24.16	1.53	−0.1777	+0.5389
EW Hβ	95.55	37.31	+0.1046	+0.0807
R λ 5007	0.26	0.22	+0.2645	+0.3446
R λ4686	0.10	0.10	−0.0765	+0.4910
R Fe II	0.55	0.38	−0.4001	−0.1164
Hβ FWHM	3777.00	1994.00	+0.3719	−0.1039
α_{ox}	1.58	0.23	−0.2097	−0.2919
Hβ shift	0.00	0.07	+0.0083	−0.0987
Hβ shape	1.16	0.09	−0.0774	−0.2887
Hβ asymm	−0.01	0.10	−0.3311	−0.1004
$M_{[OIII]}$	−27.02	1.62	−0.4137	+0.2030
Peak2 λ5007	1.04	1.17	+0.3760	+0.1887
Log R	−0.04	1.23	+0.3333	−0.2317

Table 2. Linear Correlation Coefficients between Principal Components, M_{BH} and L/L_{Edd}

	L/L_{Edd}	log M_{BH}	PC1[a]	PC2[a]	PC1[b]	PC2[b]	PC1[c]	PC2[c]
L/L_{Edd}	1.00	−0.56	0.53	−0.04	0.45	0.04	0.45	−0.07
log M_{BH}	-0.56	1.00	−0.67	−0.57	−0.56	0.60	−0.47	−0.48
PC1[a]	0.53	−0.67	1.00	0.00	0.99	−0.08	0.92	0.17
PC2[a]	−0.04	−0.57	0.00	1.00	−0.09	−0.99	−0.22	0.88
PC1[b]	0.45	−0.56	0.99	−0.09	1.00	0.00	0.99	0.11
PC2[b]	0.04	0.60	−0.08	−0.99	0.00	1.00	0.13	−0.91
PC1[c]	0.45	−0.47	0.97	−0.22	0.99	0.13	1.00	0.00
PC2[c]	−0.07	−0.48	0.17	0.88	0.11	−0.91	0.00	1.00

[a]All variables included

[b]Hβ FWHM excluded

[c]Hβ FWHM and M_V excluded